REVISED VERSION: NO 2

Seismic Wave Velocities in a Rock Body at Chalk River, Ontario: Part 1.

by

C.P. Lam * †

and

C. Wright †

Seismological Service of Canada

Internal Report # 79-9

August 1979

† Division of Seismology and Geothermal Studies

Earth Physics Branch

Department of Energy, Mines and Resources

Ottawa, Ontario, Canada

*Atomic Energy of Canada Limited

Whiteshell Nuclear Research Establishment

Pinawa, Manitoba, Canada

Abstract

Seismic velocities in a rock body believed to consist largely of gneiss and monzonite were determined along three profiles at distances up to 1.3 km radiating at azimuths of 33°, 133° and 331° from a central borehole. The overlying glacial sediments were assumed to form a different plane wedge-shaped structure beneath each profile. The seismic velocities were then estimated using recordings of the seismic energy at hydrophones in the borehole instead of the usual reversed profile technique. The solutions for the P and S wave velocities were 6.56 ± 0.30, 6.09 ± 0.30 and 5.40 ± 0.30 km/s, and 4.09 ± 0.18, 4.15 ± 0.18 and 3.18 ± 0.18 km/s respectively along each of the three profiles; the error estimates are quasi-absolute values, the calculated standard errors for the P and S wave velocities being 0.09 and 0.05 km/s respectively. The P wave velocities for two profiles are significantly higher than those measured in the laboratory on samples from the borehole, whilst the comparatively slow travel times to the southeast of the borehole suggest a change in lithology below the profiles to the northeast and northwest. The seismic sources used were a mechanical hammer and a shear wave gun.

Introduction

Elastic wave velocities in near-surface rocks are controlled primarily by pore fluids and the concentration and geometry of cracks, joints and other pore space. Further knowledge of these fracture parameters is of primary importance in assessing the value of a crystalline rock body as a potential radioactive waste disposal site. Therefore, in principle, the use of seismological techniques to determine these fracture parameters is both logical and appealing. The practical application of seismology, however, depends both on the existence of realistic mathematical models of cracked solids and on the existence of an efficient generator of shear waves (Wright, 1979a, Wright and Langley, 1979). For example, from the theory of O'Connell and Budiansky (1974), it is evident that the accurate measurement of P and S wave velocities in a rock body enables the crack density parameter and the degree of saturation to be uniquely determined.

A seismic experiment has been undertaken on a rock body believed to consist mainly of gneiss and monzonite at Chalk River, Ontario. An important objective of this preliminary study was to test the usefulness of a mechanical "hammer" as a generator of P waves and a shear wave gun as a source of S wave energy. Secondary objectives were to determine the P and S wave velocities of the rocks below the glacial sediments and to detect any significant lateral variations or anisotropy over a distance of about 1 kilometre. Another major objective, which will be discussed in a later report (Wright, 1979b), was to determine whether or not there is a measurable change of seismic velocities or attenuation in the rock body caused by the small stress changes due to the solid earth tide.

In this experiment, the usual method of reversing profiles was not used. Instead, a single shot point was utilized for each profile, and the velocities within the rock body were estimated using a line of geophones placed on the surface and hydrophones situated at depth in the borehole. Consequently, a brief description of the procedure and a summary of the mathematical derivations is included. The method used has the advantage that estimates of elastic wave velocities below the extensively fractured and weathered layer can be obtained even though the source is only about one kilometre from the most distant recorder.

Seismic Sources

Seismic energy was generated by a mechanical hammer and a shear wave gun. The hammer was originally developed by Cemetery Maintenance Incorporated, Michigan, as a special purpose pile driver for knocking the head stones of graves into the ground, and is shown in Figure 1. The weight used was about 1500 kg, which dropped a vertical distance of about 2.4 m. The shear wave gun, illustrated in Figure 2, was designed by the Environmental Research Institute of Michigan; it consisted of a four-inch mortar securely bolted on to a concrete cylinder set into the ground. The barrel of the gun was tamped by filling it with water enclosed in a plastic bag within a cardboard cylinder. The gun was fired in either of the two directions normal to the line of the recorders to give left or right polarisation of the shear wave.

Experimental Procedure

Fig. 3 shows a map of the experimental site. The borehole is situated close to a small lake north of Maskinonge Lake. The stars marked 1, 2 and 3

denote the shot locations at distances of about 1170, 1300 and 840 m from the borehole, respectively. The geophones, shown as X's on the map, were placed approximately at 100 metre intervals along each profile. A three-component set of seismometers was also present next to the borehole. In addition, a string of twelve hydrophones spaced at 10 metre intervals was placed in the borehole. Table 1A in the appendix gives the distance and elevation of each geophone with respect to the corresponding shot point for all the profiles. The origin time of each shot was recorded by an accelerometer placed next to the energy source. The sources were operated at a single shot point over a period of 24 hours, the shear wave gun firing during daylight hours and the hammer operating during the night; six shots were recorded during each hour. Thus, the total recording period was 3 days, since three shot points were used.

Table 1 shows the number of files and time period over which each geophone-source configuration was operated. Table 2A in the appendix gives the horizontal distances and vertical depths of the hydrophones below the corresponding shot point.

Mathematical Modelling

For a two dimensional dipping structure, the P or S wave velocity, the dip angle and the depth of the underlying medium beneath the shot point can be determined uniquely if a reversed profile is available (Dobrin, 1960, pp. 81-86). In the absence of a reversed profile, an additional ray path must be used. The refracted ray path of the seismic energy from the shot point to a hydrophone was used in this analysis. Figure 4 shows the ray path of a seismic wave for a plane dipping layer between a horizontal uppermost layer and an infinite half space. S_i is the shot location and R_j is the

location of the receiver. V_1 and V_2 are the P (or S) wave velocities in the upper and lower media respectively. h_i and h_j are the respective perpendicular distances from S_i and R_j on to the interface. Δ_{ij} is the horizontal distance between the shot point and the receiver. θ is the dip angle of the interface and β is the critical refraction angle.

By Snell's Law, $\sin\beta = V_1/V_2$ (1).

The apparent velocity, u, for an interface dipping from the receiver towards the source is given by

$$u = \frac{V_1}{\sin(\beta-\theta)} \qquad (2).$$

Using equations (1) and (2),

$$u = \frac{V_1 V_2}{V_1\cos\theta - \sqrt{V_2^2 - V_1^2}\sin\theta} \qquad (2').$$

From (2'), the dip angle is given by

$$\cos\theta = \frac{V_2/u + \sqrt{(V_2^2/V_1^2 - 1)(V_2^2/V_1^2 - V_2^2/u^2)}}{V_2^2/V_1^2} \qquad (3).$$

The travel time, t_{ij}, for the path S_iABR_j is as follows:

$$t_{ij} = \frac{\Delta_{ij}\sin(\beta-\theta)}{V_1} + \frac{2h_i\cos\beta}{V_1} \qquad (4),$$

where $$h_i = \frac{T_{in} V_1 V_2}{2\sqrt{V_2^2 - V_1^2}} \quad (5).$$

T_{in} is the intercept time on the time-distance plot.

To account for the difference in elevation between the shot point and the receiver, the receiver is assumed to be placed at T_j, a horizontal distance Δ'_{ij} from S_i and a vertical distance ϵ_j below S_iR_j. Then,

$$\Delta_{ij} = \Delta'_{ij} + \epsilon_j \tan(\beta - \theta) \quad (6),$$

and the travel time, t'_{ij}, along S_iABT_j, is given by

$$t'_{ij} = \frac{\Delta'_{ij} \sin(\beta - \theta)}{V_1} + \frac{2h_i \cos\beta}{V_1} - \frac{\epsilon_j}{V_1} \cos(\beta - \theta) \quad (7).$$

Thus if the travel time, t'_{ij}, is measured at T_j, both a distance correction $\delta\Delta_{ij}$ and a corresponding travel time correction δt_{ij} must be applied if the intercept time at S_i is to be found by the usual least-squares method. These corrections are given by the following two equations:

$$\delta\Delta_{ij} = \epsilon_j \left[\frac{V_1 \cos\theta - \sqrt{V_2^2 - V_1^2} \sin\theta}{V_1 \sin\theta + \sqrt{V_2^2 - V_1^2} \cos\theta} \right] \quad (8),$$

$$\delta t_{ij} = \frac{\epsilon_j V_2}{V_1 (V_1 \sin\theta + \sqrt{V_2^2 - V_1^2} \cos\theta)} \quad (9).$$

Figure 5 shows the refracted ray path from the shot point to the hydrophone, which is assumed to be within the lower medium. Symbols used are the same as in Figure 4. In addition, α is the angle of incidence and γ is the angle of refraction. d_j is the vertical distance of the hydrophone below the shot point.

The travel time, T_{ij}, between the shot point and the hydrophone is given by

$$T_{ij} = \frac{h_i}{V_1 \cos\alpha} + \frac{d_j \cos\theta - h_i + \Delta_{ij} \sin\theta}{V_2 \cos\gamma} \qquad (10).$$

The angle of refraction, γ, is given by

$$\tan\gamma = a - \frac{b\frac{V_1}{V_2}\sin\gamma}{(1 - V_1^2 \sin^2\gamma / V_2^2)^{\frac{1}{2}}} \qquad (11),$$

where

$$a = \frac{\Delta_{ij}\cos\theta - d_j \sin\theta}{d_j\cos\theta - h_i + \Delta_{ij}\sin\theta} \qquad (12),$$

and

$$b = \frac{h_i}{d_j\cos\theta - h_i + \Delta_{ij}\sin\theta} \qquad (13).$$

The angle of incidence, α, can then be obtained by Snell's Law, as follows:

$$\frac{\sin\alpha}{\sin\gamma} = \frac{V_1}{V_2} \qquad (14).$$

Data Reduction

The total number of individual 24-trace seismic records is 445, which can be divided into nine groups: one group for each location of the mechanical hammer and two (left and right polarization) for each location of the shear wave gun. Stacking of the individual records from the same group enabled the signal-to-noise ratios to be increased. Noting that the left and right records for the shear wave gun differ only on horizontal component instruments, six master sets of stacked seismograms were obtained: three for the hammer and three for the shear wave gun.

Figures 6 to 10 show sample seismograms. Figures 6, 7 and 8 are the seismograms of the individual records for the mechanical hammer and right and left polarization of the shear wave gun, while Figures 9 and 10 are the stacked seismograms of the mechanical hammer and the shear wave gun. It is obvious from these figures that the signals of the stacked seismograms are much less noisy than those of the individual records.

To determine the P or S wave velocity of the lower medium, the travel times were picked from the stacked seismograms. Table 3A of the appendix gives the travel times for all the profiles. Figures 11 and 12 show the travel time-distance plots for P and S wave data respectively. A least-squares straight line was fitted to each time-distance plot to determine the apparent velocity of the lower medium. Table 2 gives the values of the reciprocal slope, time intercept and the P and S wave travel times at the second lowermost hydrophone for all three profiles. The P or S wave velocity and the dip angle were calculated for each profile by using the refracted ray path from the shot point to the hydrophone in the following manner. By assuming velocities in the upper and lower media, the dip angle of the

interface was determined by equation (3) using the calculated apparent velocity, u. The perpendicular distance from the shot point to the interface was then computed from equation (5). The angle of refraction, γ, was determined numerically with equation (11), and the angle of incidence was determined with equation (14). The travel time from the shot point to the hydrophone was then calculated by equation (10). With a range of velocities in the upper and lower media, a suite of travel times was calculated. A series of solutions was obtained by matching the computed travel time with the corresponding measured travel time. Whenever there was a significant difference in elevation between the shot point and the geophone location, corrections were calculated from equations (8) and (9) using approximate values of V_1, V_2 and θ obtained from the uncorrected travel times. A corrected set of travel times and offset distances was then obtained from which a new apparent velocity and time intercept were derived. The velocity in the lower medium was then determined by the procedure described above.

Results

Assuming a plane dipping interface between sediments and the underlying crystalline rock body, a range of seismic velocities in the upper and lower media can satisfy the measured travel time for a refracted ray path from the shot point to the hydrophone. The range of solutions for the P and S wave velocities as well as the dip angle of the interface and overburden thickness below the shot point for all the profiles are listed in Tables 4-7. The calculated P wave velocities in the lower medium ranged from 6.54 to 6.58, 6.07 to 6.11 and 5.38 to 5.43 km/s for profiles 1, 2 and 3 respectively. The values of S wave velocity in the lower medium range from 4.08 to 4.11, 4.13 to

4.17 and 3.15 to 3.20 km/sec for profiles 1, 2 and 3 respectively. Figures 13 and 14 show the range of dipping structures and the corresponding profiles of the surface topography for P and S waves respectively. An analysis of the errors in the seismic velocities is given in the appendix; for P and S velocities the overall errors are about 0.30 and 0.18 km/s respectively.

Discussion

Travel-time anomalies

Seismograms along the three profiles indicate that there are a number of travel-time anomalies. The early arrival time (both P and S wave) at the geophone placed 510 meters from shot point 1 (Figure 11) suggests that there might be a thinning of the sedimentary cover around that region. Subsequently, this location was not used in determining the least-squares straight line for profile 1. Separation of the travel time-distance relation along profile 2 into two straight lines of similar slopes with a time offset indicates that there might be an abrupt thickening of the sediments perhaps indicating a fault between 330 and 420 m from the shot point. The data for profile 1 suggest that the P velocity within the overburden close to shot point 1 is about 3.0 km/s.

P and S wave velocities

It is clear that to the northwest and northeast of the borehole of Figure 3, the average seismic velocities are high, the P wave velocities being in excess of 6.0 km/s; in contrast, the velocities to the southeast of the borehole are low. The borehole P velocity log from the Geological Survey of

Canada and the laboratory values of P and S wave velocities obtained by Simmons, Batzle and Cooper (1978) are in the range 4.9-6.3 km/s and 3.0-3.6 km/s respectively for the gneisses and monzonites of the drill cores. We suggest that the rocks beneath profile 3 are of the same type as the cores from the borehole. The slightly lower velocities of about 5.5 km/s may be because the ray paths to the hydrophones are partly through the extensively weathered and fractured region immediately below the sediments. If we make the rather extreme assumption that the slow travel times of profile 3 are due to a basin of low velocity sediments immediately beneath the shot point, we obtain an upper bound of 5.9 km/s for the P wave velocity in the underlying rock body.

The results for profiles 1 and 2 seem to present greater ambiguities in interpretation. The cores from the borehole that are likely to give the highest seismic velocities are petrographically monzonite, verging on syenite, and they occur at depths between 90 and 170 m. Smithson and Shive (1975) reported in situ P wave velocities in the range 6.0-6.4 km/s at depths down to 1.3 km in a syenite body. The P velocity for profile 1 therefore seems too high to be explained in terms of the rock types from the borehole. Moreover, another borehole to the northwest of the present one intersected 80 m of gabbro. We suggest that the P wave velocity of 6.56 km/s along profile 1 corresponds to propagation through gabbroic material along a substantial portion of the ray path. The presence of gabbro beneath profile 2 is also a plausible explanation of the velocities in excess of 6.0 km/s.

The Seismic Sources

The hammer provides a good and reasonably cheap source of P wave energy at distances up to at least one kilometre. The shear wave gun gave distinct S wave arrivals only along profile 1. We suggest that the rigidity of the overburden at shot points 2 and 3 was too small to effectively transmit shear stresses. The shear wave gun would only be worth further testing as a source of shear wave energy if the cost of running it could be reduced considerably. At present, it is prohibitively expensive.

Recommendations for Future Work

Our recommendations for future work are based on four separate considerations: (a) structural detail and network configuration, (b) source properties, (c) mathematical theories of cracked solids, and (d) supportive laboratory studies.

(a) Our concern in this report is not primarily with the amount of detailed information that can be obtained from refraction surveys, but with employing techniques that may be relevant to the calculation of crack parameters. The variations of velocity along profiles 2 and 3 have been studied using the seismic reflection data described in the report by Mair and Lam (1979), and the results extracted from an elaborate configuration of recorders and shot points have been discussed by Wright, Johnston and Lam (1979). The important point to emphasize here is that with the station configuration used in this experiment, the random errors in velocities that have been derived in the appendix are about 1.5%.

(b) It is now possible to use the weight drop device in the shear mode, and further tests with this modified hammer as a possible shear wave generator appear to be worthwhile. The modified hammer can be expected to provide P and S wave arrivals at distances up to at least 500 m. A trial experiment should be conducted in which the source is placed both on glacial overburden and on rock outcrops. Surface recording should include both vertical and transverse horizontal-component phones, whilst a three-component lock-in phone should be placed in a borehole within 500 m of the source. The testing of the shear wave source is envisaged as the initial phase of any future program. If useful shear wave arrivals are not obtained, alternative sources of shear wave energy should be tested before proceeding with the second phase that involves the accurate measurement of seismic velocities and attenuation.

(c) Recent progress in the development of mathematical theories of the elastic properties of cracked solids and its relevance to the 'RADWASTE' program has been outlined by Wright and Langley (1979). In particular, the work of O'Connell and Budiansky (1977) has demonstrated the existence of quantitative relationships between seismic velocities, elastic wave attenuation, crack parameters, porosity and permeability. Therefore, in the second phase of the proposed experiments, an attempt to obtain seismic attenuation measurements using recording both on the surface and in a borehole should be made.

(d) The effective use of crack theories in the interpretation of field data requires the existence of both P and S wave velocity measurements in

the laboratory at pressures up to at least 2.0 kb, and the availability of modal and petrofabric analyses of the cores (Wright and Langley, 1979). These laboratory studies thus provide data that are essential for the use of mathematical theories in determining crack parameters.

References

Dobrin, M.B, Introduction to Geophysical Prospecting, 435 pp., McGraw Hill, New York, 1960.

Mair, J.A., and C.P. Lam, Seismic Lateral Studies; high resolution seismic reflection project, Internal report 79-1, 7pp. Seismological Service of Canada, Department of Energy, Mines and Resources, Ottawa, February, 1979.

O'Connell, R.J., and B. Budiansky, Seismic velocities in dry and saturated cracked solids, J. Geophys. Res., 79, 5412-5426, 1974.

O'Connell, R.J., and B. Budiansky, Viscoelastic properties of fluid-saturated cracked solids, J. Geophys. Res., 82, 5719-5735, 1977.

Simmons, G., M.L. Batzle and H. Cooper, The characteristics of microcracks in several igneous rocks from the Chalk River Site: Final Report, 40 pp., Department of Energy, Mines and Resources, 1 July, 1978.

Smithson, S.B. and P.N. Shive, Field measurements of compressional wave velocities in common crystalline rocks, Earth and Planetary Science Letters 27, 170-176, 1975.

Wright, C., On the justification of seismological studies as part of the 'RADWASTE' program, (unpublished report), 16 pp., 1979a.

Wright, C., The search for temporal changes in seismic velocities at Chalk River, Ontario, Internal Report 79-11, 6 pp., Seismological Service of Canada, Department of Energy, Mines and Resources, Ottawa, August, 1979.

Wright, C. and K. Langley, Estimates of crack-density parameters in near-surface rocks from laboratory studies of core samples and in-situ seismic velocity measurements, Internal Report 79-7 , 21 pp., Seismological Service of Canada, Department of Energy, Mines and Resources, Ottawa, August, 1979.

Wright, C., M. Johnston and C.P. Lam, Seismic wave velocities in a rock body at Chalk River, Ontario: Part 2, Internal Report No. 79-10, 10 pp., Seismological Service of Canada, Department of Energy, Mines and Resources, Ottawa, August, 1979.

Appendix

n this appendix we have given an outline of the error theory used to calculate the random errors in the velocity solutions for the rock body. In addition, three extra tables of data are presented: (i) the horizontal distances and elevations of the shot points, borehole, geophones and the three-component set of seismometers; (ii) the horizontal distance and vertical depth of the hydrophone used to derive velocities for each shot point and energy source; (iii) the P and S wave travel times to each geophone or seismometer and the corresponding distance from the shot point.

Error Analysis

From the least-squares line fitted through the travel time-distance curve, we can estimate errors on the apparent velocity and intercept time which we call δu and δT_{in} respectively. Then, by differentiation of equations (3) and (5) the errors in dip angle θ and overburden thickness h_i are given by

$$\delta\theta = \left[\frac{V_1}{V_2 u^2} - \frac{V_1^2}{u^3} \cdot \frac{\sqrt{\left(\frac{V_2^2}{V_1^2} - 1\right)}}{\sqrt{\left(\frac{V_2^2}{V_1^2} - \frac{V_1^2}{u^2}\right)}} \right] \frac{\delta u}{\sin\theta} \qquad (1A),$$

$$\delta h_i = \frac{V_1 V_2}{2\sqrt{V_2^2 - V_1^2}} \cdot \delta T_{in} \qquad (2A).$$

Differentiating equation (10) for the travel time from the shot point to a hydrophone, we obtain

$$\frac{\partial T_{ij}}{\partial h_i} = \frac{1}{V_1 \cos\alpha}\left[1 + h_i \tan\alpha \frac{\partial \alpha}{\partial h_i}\right] - \frac{1}{V_2 \cos\gamma}\left[1 - (d_j \cos\theta - h_i + \Delta_i \sin\theta)\tan\gamma \frac{\partial \gamma}{\partial h_i}\right] \quad (3A),$$

$$\frac{\partial T_{ij}}{\partial \theta} = \frac{h_i}{V_1}\frac{\tan\alpha}{\cos\alpha}\frac{\partial \alpha}{\partial \theta} + \frac{1}{V_2 \cos\gamma}\left[\Delta_i \cos\theta - d_j \sin\theta + (d_j \cos\theta - h_i + \Delta_i \sin\theta)\tan\gamma \frac{\partial \gamma}{\partial \theta}\right] \quad (4A).$$

The error in T_{ij} due to errors in h_i and θ can then be calculated using the expression

$$\delta T_{ij}^2 = \left(\frac{\partial T_{ij}}{\partial h_i}\right)^2 \delta h_i^2 + \left(\frac{\partial T_{ij}}{\partial \theta}\right)^2 \delta\theta^2 \quad (5A),$$

where δT_{ij} is the standard error on T_{ij}. To calculate $\frac{\partial T_{ij}}{\partial h_i}$ and $\frac{\partial T_{ij}}{\partial \theta}$ we must first evaluate $\frac{\partial \alpha}{\partial h_i}$, $\frac{\partial \gamma}{\partial h_i}$, $\frac{\partial \alpha}{\partial \theta}$ and $\frac{\partial \gamma}{\partial \theta}$. By differentiating equation (11), the following equations for $\frac{\partial \gamma}{\partial h_i}$ and $\frac{\partial \gamma}{\partial \theta}$ are obtained:

$$\frac{\partial \gamma}{\partial h_i} = \left[\frac{\partial a}{\partial h_i} - \frac{\partial b}{\partial h_i}\cdot\frac{\frac{V_1}{V_2}\sin\gamma}{\sqrt{1 - \frac{V_1^2}{V_2^2}\sin^2\gamma}}\right] \Bigg/ \left[\sec^2\gamma + \frac{b\frac{V_1}{V_2}\cos\gamma}{\left(1 - \frac{V_1^2}{V_2^2}\sin^2\gamma\right)^{3/2}}\right] \quad (6A),$$

$$\frac{\partial \gamma}{\partial \theta} = \left[\frac{\partial a}{\partial \theta} - \frac{\partial b}{\partial \theta}\cdot\frac{\frac{V_1}{V_2}\sin\gamma}{\sqrt{1 - \frac{V_1^2}{V_2^2}\sin^2\gamma}}\right] \Bigg/ \left[\sec^2\gamma + \frac{b\frac{V_1}{V_2}\cos\gamma}{\left(1 - \frac{V_1^2}{V_2^2}\sin^2\gamma\right)^{3/2}}\right] \quad (7A).$$

Also required are expressions for $\frac{\delta a}{\delta h_i'}$ $\frac{\delta b}{\delta h_1}$, $\frac{\delta a}{\delta \theta}$ and $\frac{\delta b}{\delta \theta}$, which can be derived from equations (12) and (13).

$$\frac{\partial a}{\partial h_i} = \frac{\Delta_i \cos\theta - d_j \sin\theta}{(d_j \cos\theta - h_i + \Delta_i \sin\theta)^2} \qquad (8A),$$

$$\frac{\partial b}{\partial h_i} = \frac{d_j \cos\theta + \Delta_i \sin\theta}{(d_j \cos\theta - h_i + \Delta_i \sin\theta)^2} \qquad (9A),$$

$$\frac{\partial a}{\partial \theta} = \frac{h_i \Delta_i \sin\theta - h_i d_j \cos\theta - \Delta_i^2 - d_j^2}{(d_j \cos\theta - h_i + \Delta_i \sin\theta)^2} \qquad (10A),$$

$$\frac{\partial b}{\partial \theta} = \frac{h_i d_j \sin\theta - h_i \Delta_i \cos\theta}{(d_j \cos\theta - h_i + \Delta_i \sin\theta)^2} \qquad (11A).$$

Differentiating equation (14),

$$\frac{\partial \alpha}{\partial \gamma} = \frac{V_1 \cos\gamma}{V_2 \cos\alpha} \qquad (12A).$$

$\frac{\partial \alpha}{\partial h_i}$ and $\frac{\partial \alpha}{\partial \theta}$ can then be calculated from $\frac{\partial \gamma}{\partial h_i}$ and $\frac{\partial \gamma}{\partial \theta}$ using equation (12A), since $\frac{\partial \gamma}{\partial h_i} = \frac{\partial \gamma}{\partial h_i} \cdot \frac{\partial \alpha}{\partial \gamma}$ and $\frac{\partial \alpha_i}{\partial \theta} = \frac{\partial \gamma}{\partial \theta} \cdot \frac{\partial \alpha}{\partial \gamma}$.

In addition to the calculated error δT_{ij}, we have an additional error due to the measurement of T_{ij}, which we call $(\delta T_{ij})_m$. Then the total error in T_{ij}, $(\delta T_{ij})_{tot}$ is given by

$$(\delta T_{ij})^2_{tot} = \left[\delta T_{ij}^2 + (\delta T_{ij})^2_m \right]^{\frac{1}{2}} \qquad (13A).$$

Having calculated $(\delta T_{ij})_{tot}$, the corresponding error in V_2 is estimated from the table of values of T_{ij} derived from equation (10) keeping V_1 constant. This procedure results in a standard error of about 0.09 km/s for the P wave velocities and ±0.05 km/s or the S wave velocities. The range of possible values of V_1 results in an additional uncertainty in V_2 of ±0.03 km/s for both P and S velocities; this additional error term may be classed as systematic. Adhering to the recommendations of Eisenhart (1968)

for quoting errors when the systematic and random errors are of similar magnitudes, we can make the following statements concerning the errors in the P and S wave velocities respectively. The overall uncertainty is ±0.30 (± 0.18) km/s, which is based on a computed standard error of 0.09(0.05) km/s and an estimated bound of ±0.03 km/s on the systematic error. The figure 0.30 (0.18) is equal to 0.03 plus 3 times 0.09(0.05), where 3 is the approximate value of Student's t for a large number of degrees of freedom exceeded in absolute value with 0.002 probability.

Reference

Eisenhart, C, Expression of the uncertainties of final results, Science, 160, 1201-1204, 1968.

TABLE 1A CHALK RIVER EXPERIMENT, OCTOBER, 1977.

1. DISTANCE MEASUREMENTS: SHOT POINTS-GEOPHONES.				2. STATION AND SHOT-POINT HEIGHTS.	
MEASUREMENT LOCATIONS	DISTANCE MEASURED ON MAP, METRES	DISTANCE FROM CHAINING, METRES	ELEVATION CHANGE, (±0.8M) METRES	STATION OR SHOT POINT	ELEVATION, METRES
SP1-1G1	93.24±0.78	92.96±0.49	-6.7	1G1	160.0
SP1-1G2	192.84±1.06	192.02±0.69	-0.6	1G2	166.1
SP1-1G3	295.20±1.29	294.13±0.85	-1.5	1G3	165.2
SP1-1G4	400.80±1.47	399.29±0.98	-4.9	1G4	161.8
SP1-1G5	510.00±1.64	507.49±1.10	-11.9	1G5	154.8
SP1-1G6	610.44±1.79	609.60±1.20	-11.9	1G6	154.8
SP1-1G7	714.00±1.93	713.23±1.30	-16.7	1G7	150.0
SP1-1G8	814.20±2.06	815.34±1.39	-22.2	1G8	144.5
SP1-DH	1167.24±2.18	1172.87±1.70	-42.7		
SP1-3CS	1168.08±2.30	---	-43.0	SP1	166.7
SP2-2G1	90.48±1.27	---	-5.2	2G1	121.3
SP2-2G2	187.03±1.46	---	-7.9	2G2	118.9
SP2-2G3	288.31±1.63	---	-8.2	2G3	118.6
SP2-2G4	333.05±1.78	---	-6.1	2G4	120.7
SP2-2G5	421.85±1.92	---	-6.7	2G5	120.1
SP2-2G6	516.72±2.05	---	-4.6	2G6	122.2
SP2-2G7	5[illegible].60±2.18	---	-5.5	2G7	121.3
SP2-2G8	[illegible]3.68±2.29	---	-2.7	2G8	124.1
SP2-DH	1301.40±2.41	---	-1.8		
SP2-3CS	1306.68±2.51	---	-2.1	SP2	126.8*
SP3-3G1	98.52±1.29	---	3.4	3G1	132.0
SP3-3G2	197.88±1.47	---	1.9	3G2	130.5
SP3-3G3	297.96±1.64	---	-2.4	3G3	126.2
SP3-3G4	399.84±1.79	---	-6.7	3G4	121.9
SP3-3G5	500.16±1.93	---	-8.8	3G5	119.8
SP3-3G6	600.12±2.06	---	-10.6	3G6	118.0
SP3-3G7	703.56±2.18	---	-9.4	3G7	119.2
SP3-DH	843.48±2.41	---	-3.6		
SP3-3CS	838.32±2.51	---	-3.9	SP3	128.6
SP4-DH	486.48±2.06	---	0.0	SP4	125.0
SP4-3CS	490.92±2.18	---	-0.3		
				DH	125.0
				3CS	124.7

TABLE 2A) HORIZONTAL DISTANCE AND VERTICAL DEPTH OF THE HYDROPHONE USED TO DERIVE VELOCITIES FROM THE SHOT POINT FOR EACH CONFIGURATION AND ENERGY SOURCE.

PROFILE	ENERGY SOURCE	HORIZONTAL DISTANCE, (M)	VERTICAL DEPTH, (M)
1	HAMMER	1131.47	255.15
	SHEAR WAVE GUN	1145.91	155.80
2	HAMMER	1280.38	117.04
	SHEAR WAVE GUN	1280.38	117.04
3	HAMMER	860.04	118.84
	SHEAR WAVE GUN	860.04	118.84

TABLE 3A) P AND S WAVE TRAVEL TIMES AND DISTANCES.

PROFILE 1			PROFILE 2			PROFILE 3		
OFFSET DISTANCE, (M)	P WAVE TRAVEL TIME, (MS)	S WAVE TRAVEL TIME, (MS)	OFFSET DISTANCE, (M)	P WAVE TRAVEL TIME, (MS)	S WAVE TRAVEL TIME, (MS)	OFFSET DISTANCE, (M)	P WAVE TRAVEL TIME, (MS)	S WAVE TRAVEL TIME, (MS)
93.24	25.00	55.75	90.48	42.00	52.50	98.52	70.00	101.25
295.20	79.67	108.31	288.31	60.90	82.50	297.96	96.00	---
400.80	90.63	131.87	333.05	71.87	92.50	399.84	113.10	191.25
510.00	9[illegible]	15[illegible].87	421.85	103.12	151.25	500.16	131.00	213.75
610.44	11[illegible]	17[illegible].75	516.72	---	162.50	600.12	148.70	253.75
814.20	146.[illegible]	227.50	673.68	131.25	190.00	703.56	165.00	---
1168.08	200.00	290.00	1306.68	212.00	283.75	838.32	181.60	---
	(A)	(B)		(C)	(D)		(E)	(F)

(A) = FILES 197-240 STACKED.
(B) = FILES 150-174 STACKED (RIGHT POLARISATION).
(C) = FILES 381-429 STACKED.
(D) = FILES 291-331 STACKED (LEFT POLARISATION).
(E) = FILES 53- 97 STACKED.
(F) = FILES 4- 52 STACKED (LEFT POLARISATION).

Figure Captions

Figure 1 The mechanical hammer.

Figure 2 The shear wave gun.

Figure 3 Map showing the locations of the shot points, receivers and borehole CR1, near Chalk River, Ontario.

Figure 4 Geometrical ray path representation of a head wave travelling along a dipping interface between a horizontal uppermost layer and an infinite half space.

Figure 5 Refracted ray path between a shot point on the surface and a hydrophone in a borehole, assuming a plane dipping interface between the overburden and the underlying crystalline rock body.

Figure 6 Seismograms generated by a single 'shot' from the mechanical hammer.

Figure 7 Seismograms generated by a single 'shot' from the shear wave gun (right polarization).

Figure 8 Seismograms generated by a single 'shot' from the shear wave gun (left polarization).

Figure 9 Stacked seismograms (51 files) from the mechanical hammer

Figure 10 Stacked seismograms (15 files) from the shear wave gun (left polarization).

Figure 11 Travel time versus distance plots for the P wave arrivals along profiles 1 (top), 2 (middle) and 3 (bottom).

Figure 12 Travel time versus distance plots for the S wave arrivals along profiles 1 (top), 2 (middle) and 3 (bottom).

Figure 13 Vertical sections along the profiles and range of allowable dipping structures as interpreted from P wave arrivals generated by the mechanical hammer.

Figure 14 Vertical sections along the profiles and range of allowable dipping structures as interpreted from S wave arrivals generated by the shear wave gun.

Table 1: List of File numbers with Period of Operation for Each Geophone - Source Configuration

File Numbers	Location (as shown in Figure 3)	Energy Source	Period of Operation (Eastern Standard Time)
1-52	3	Shear Wave Gun	October 14, 1977, 10:55 - 17:34
53-145	3	Hammer	October 14, 1977, 22:48- 13:15, October 15, 1977
147-182	1	Shear Wave Gun	October 15, 1977, 13:15 - 17:59
184-290	1	Hammer	October 15, 1977, 20:26- 09:15, October 16, 1977
291-335	2	Shear Wave Gun	October 16 1977, 12:00 - 18:25
336-429	2	Hammer	October 16, 1977, 20:55- 09:10, October 17, 1977
430-437	2	Shear Wave Gun	October 17, 1977, 10:12 - 10:25
438-445	4*	Shear Wave Gun	October 17, 1977, 12:41 - 13:12

* Shot point 4 is not shown in Figure 3; it was 486.5 m from the drill hole along profile 2.

Table 2: Apparent Velocities, Intercept Times and Travel Times to One Hydrophone for Both P and S Waves.

Energy Source	Profile	Apparent Velocity, km/s	Intercept Time, ms	Travel Time at Second Lowermost Hydrophone, ms
Mechanical	1	7.21	35.90	193.6
Hammer	2	8.71*	31.02	225.0
	3	5.89	45.83	181.8
Shear Wave	1	4.70	41.78	301.25
Gun	2	6.22*	37.66	326.8
	3	3.37	71.23	305.6

* For three phones nearest to the shot point.

Table 3: Range of Solutions for the P Wave Velocities in the Upper and Lower Media, Thickness of Overburden and Dip Angle of Interface

	Velocity in Upper Medium, km/s	Velocity in Lower Medium, km/s	Thickness of Overburden below Shot Point, m	Dip Angle of Interface, deg
	3.375	6.51	70.96	3.32
	3.125	6.52	64.00	2.95
Profile 1	2.825	6.53	56.30	2.57
	2.525	6.54	49.17	2.21
	2.175	6.55	41.41	1.84
	1.825	6.56	34.12	1.49
	1.425	6.57	26.21	1.13
	3.275	6.07	61.37	10.57
Profile 2	3.025	6.08	54.84	9.51
	2.725	6.09	47.77	8.35
	2.375	6.10	40.30	7.09
	1.975	6.11	32.53	5.75
	3.225	5.38	92.51	3.63
	3.000	5.39	82.88	3.20
Profile 3	2.725	5.40	72.41	2.75
	2.400	5.41	61.44	2.29
	2.025	5.42	50.05	1.83
	1.600	5.43	38.38	1.37

Table 4: Range of Solutions for the P Wave Velocities in the Upper and Lower Media, Thickness of Overburden and Dip Angle of Interface

	Velocity in Upper Medium, km/s	Velocity in Lower Medium, km/s	Thickness of Overburden below Shot Point, m	Dip Angle of Interface, deg
	3.050	6.54	63.51	2.32
	2.750	6.55	55.80	2.00
Profile 1*	2.425	6.56	48.06	1.69
	2.075	6.57	40.26	1.39
	1.700	6.58	32.39	1.10

* Revised solution incorporating elevation corrections for the geophone arrival times.

Table 5: Range of Solutions for the S Wave Velocities in the Upper and Lower Media, Thickness of Overburden and Dip Angle of Interface

	Velocity in Upper Medium, km/s	Velocity in Lower Medium, km/s	Thickness of Overburden below Shot Point, m	Dip Angle of Interface, deg
	2.500	4.08	66.41	5.55
Profile 1	2.175	4.09	53.82	4.56
	1.775	4.10	41.21	3.46
	1.200	4.11	26.23	2.18
	2.325	4.13	54.22	12.31
	2.050	4.14	45.18	10.44
Profile "	1.700	4.15	35.46	8.32
	1.250	4.16	24.81	5.89
	1.600	4.17	11.43	2.74
	2.425	3.15	135.71	4.32
	2.275	3.16	116.97	3.59
Profile 3	2.050	3.17	95.84	2.83
	1.750	3.18	74.70	2.10
	1.350	3.19	53.08	1.42
	0.825	3.20	30.41	0.77

Table 6: Range of Solutions for the S Wave Velocities in the Upper and Lower Media, Thickness of Overburden and Dip Angle of Interface

	Velocity in Upper Medium, km/s	Velocity in Lower Medium, km/s	Thickness of Overburden below Shot Point, m	Dip Angle of Interface, deg
	2.550	4.10	72.47	4.37
Profile 1*	2.225	4.11	58.83	3.50
	1.775	4.12	43.69	2.56
	1.150	4.13	26.58	1.53

* Revised solution incorporating elevation corrections for the geophone arrival times.

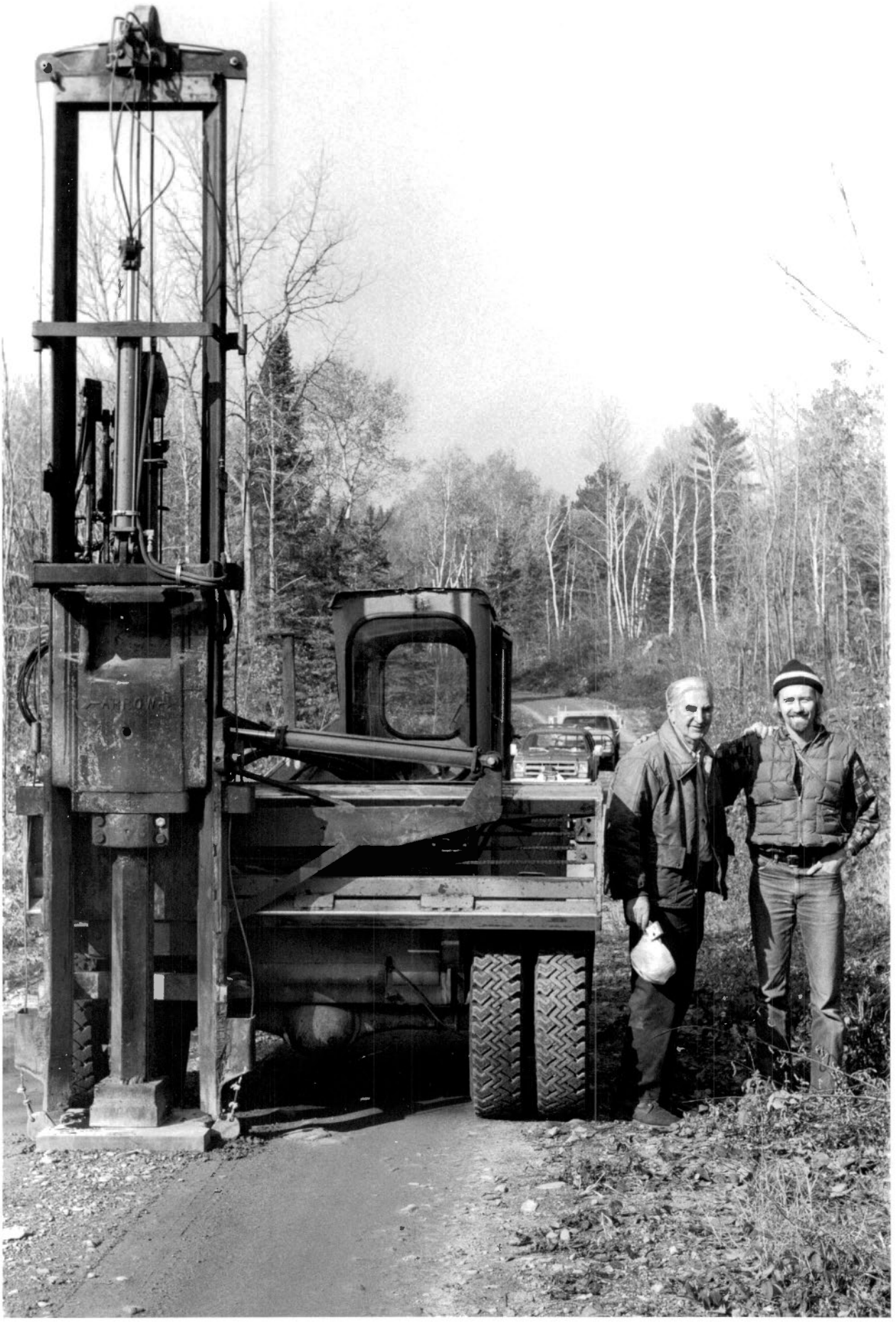

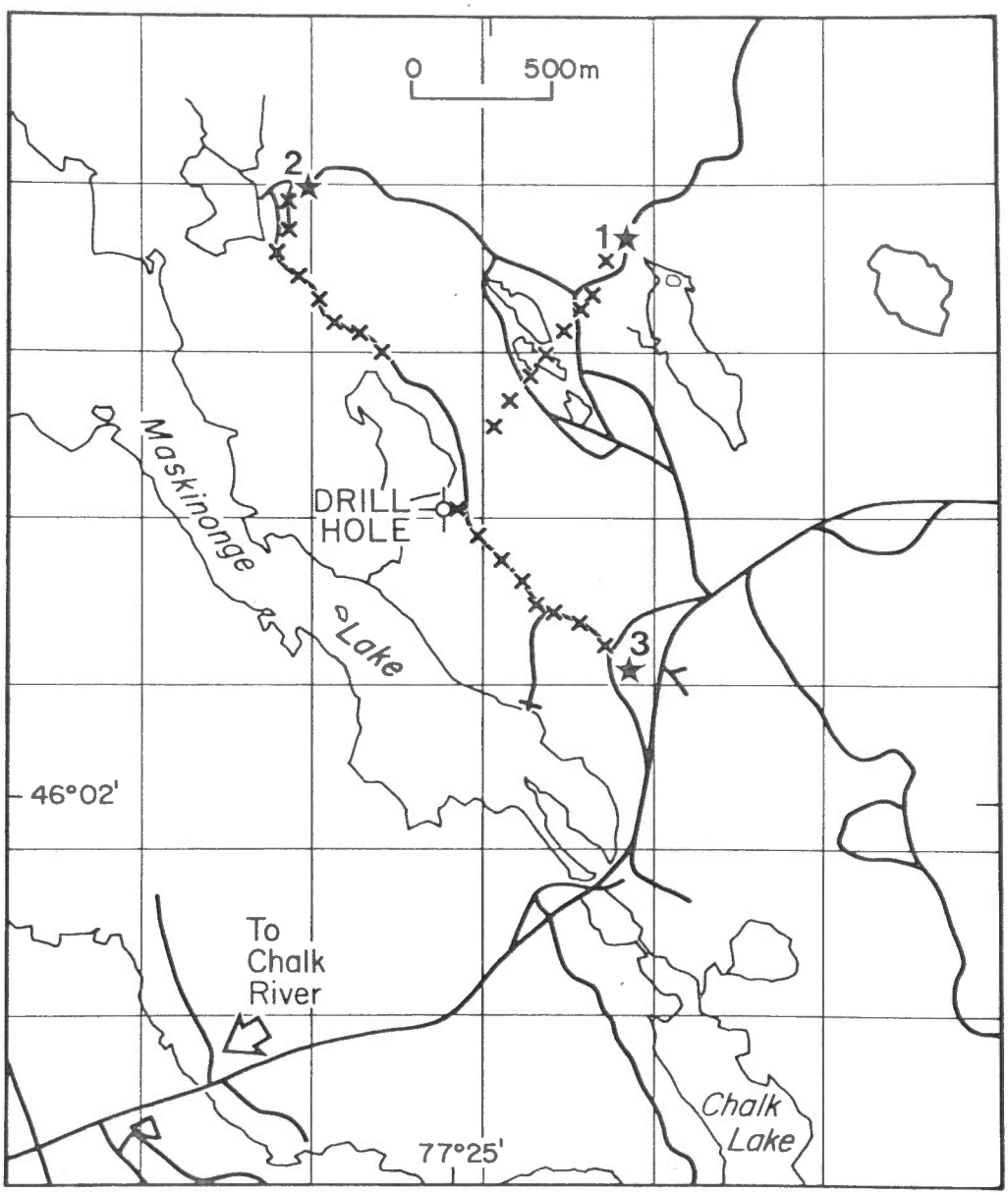
0
500m
2
1
3
DRILL HOLE
Maskinonge Lake
46°02'
To Chalk River
77°25'
Chalk Lake

FIG. 3

Fig. 4

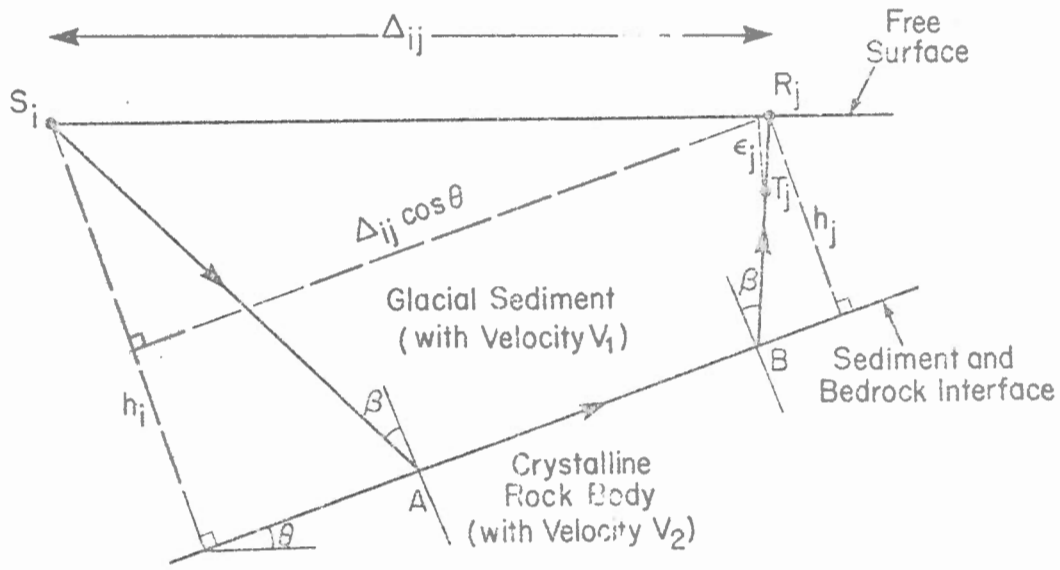
Δ_{ij}
Free Surface
S_i
R_j
ϵ_j
T_j
h_j
$\Delta_{ij}\cos\theta$
β
Glacial Sediment
(with Velocity V_1)
h_i
β
B
Sediment and Bedrock Interface
A
Crystalline Rock Body
(with Velocity V_2)
θ

Fig 5

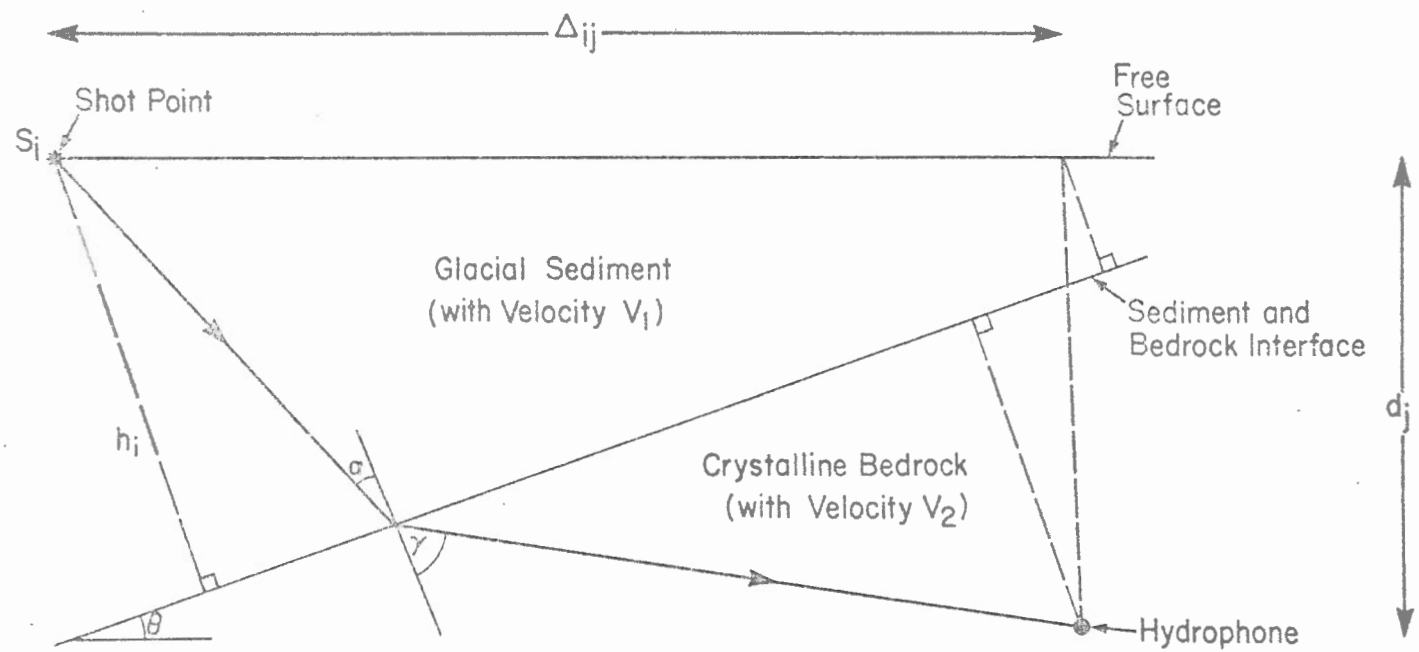
Δ_{ij}
Shot Point
S_i
Free Surface
Glacial Sediment
(with Velocity V_1)
Sediment and Bedrock Interface
h_i
σ
Crystalline Bedrock
(with Velocity V_2)
γ
θ
Hydrophone
d_j

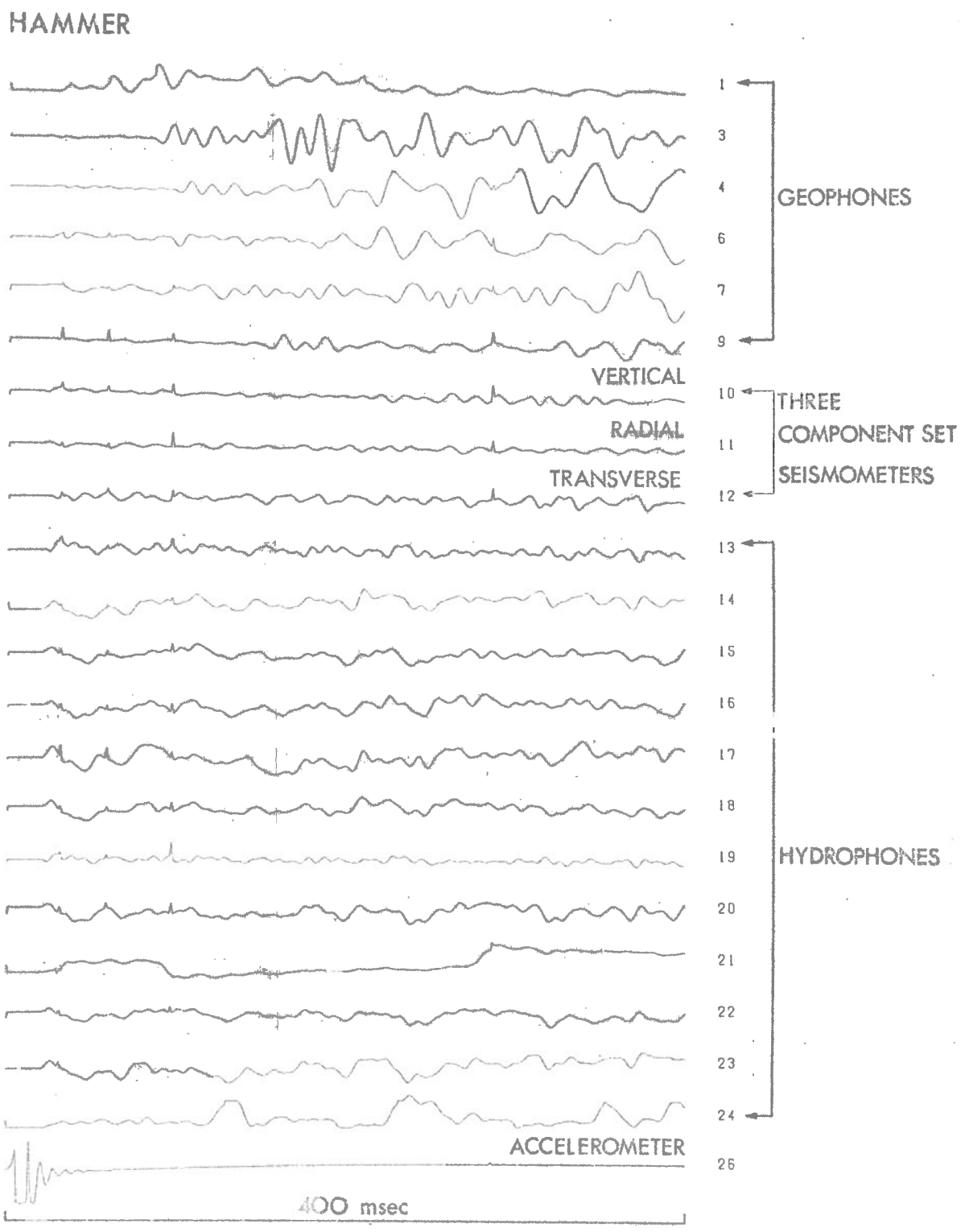
HAMMER
1
3
4
6
7
9
GEOPHONES
VERTICAL
RADIAL
TRANSVERSE
10
11
12
THREE
COMPONENT SET
SEISMOMETERS
13
14
15
16
17
18
19
20
21
22
23
24
HYDROPHONES
ACCELEROMETER
26
400 msec

Fig. 6

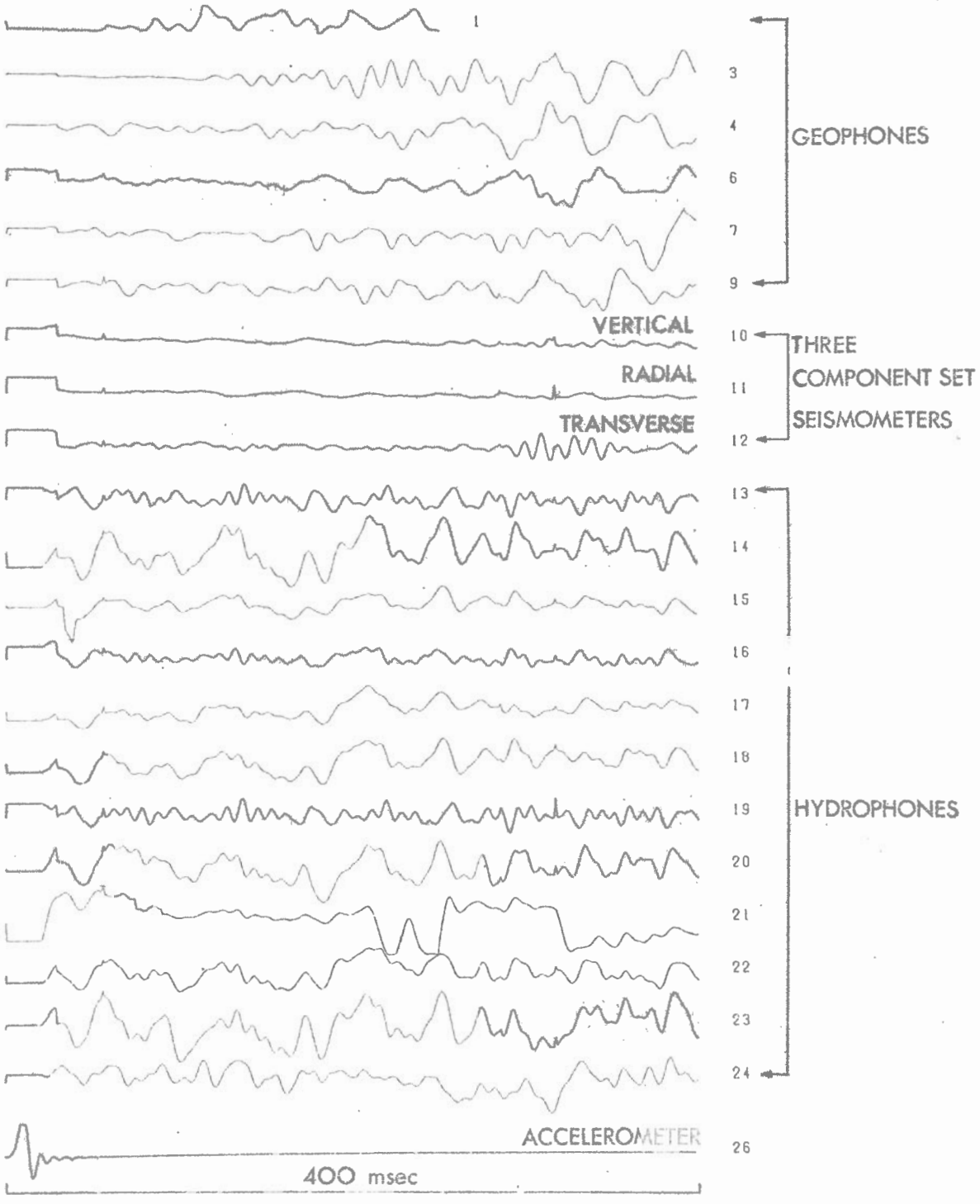
SHEAR WAVE GUN (RIGHT)
1
3
4
6
7
9
GEOPHONES
VERTICAL
RADIAL
TRANSVERSE
10
11
12
THREE
COMPONENT SET
SEISMOMETERS
13
14
15
16
17
18
19
20
21
22
23
24
HYDROPHONES
ACCELEROMETER
26
400 msec

FIG. 7

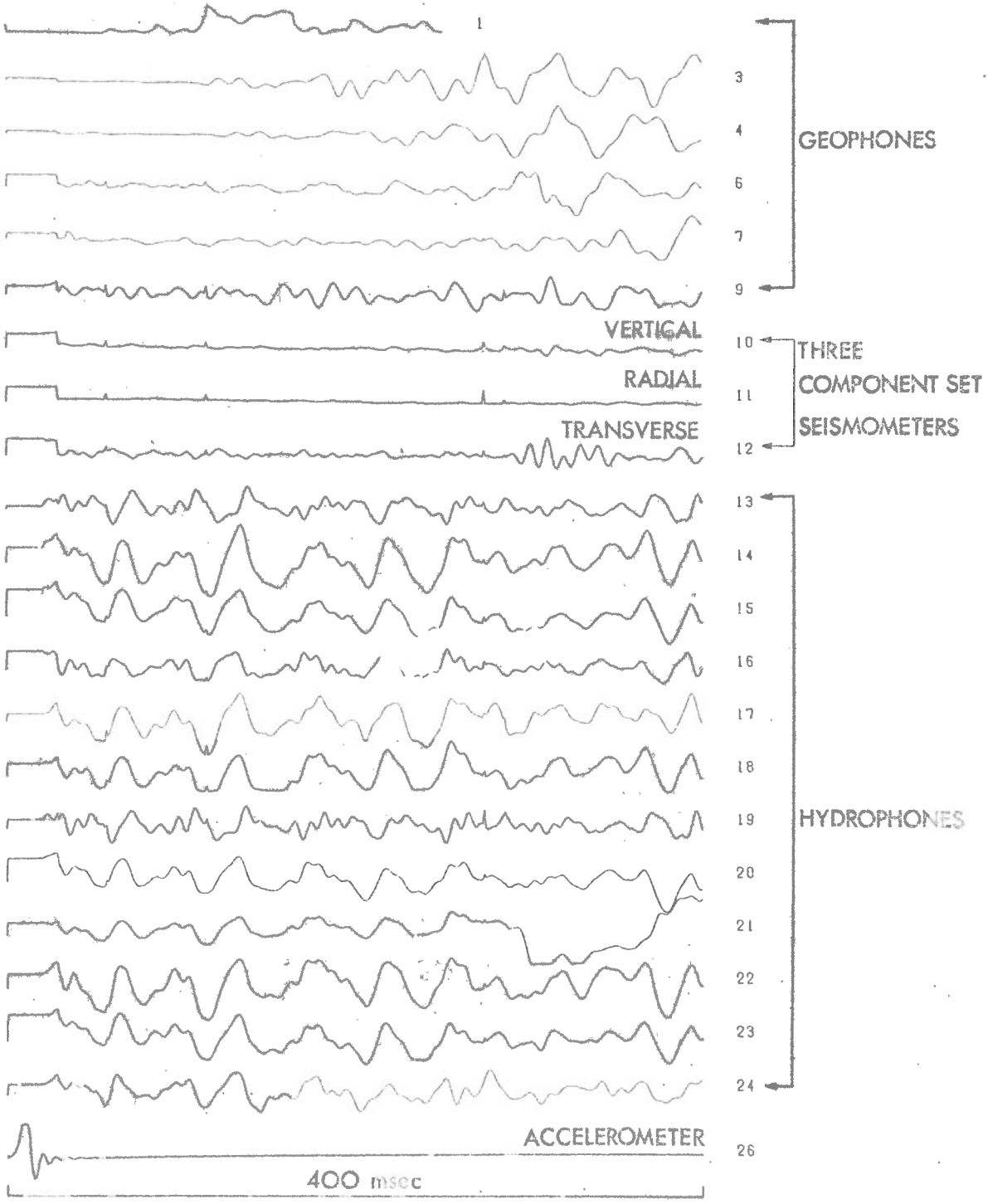
SHEAR WAVE GUN (LEFT)
1
3
4
6
7
9
GEOPHONES
VERTICAL
RADIAL
TRANSVERSE
10
11
12
THREE
COMPONENT SET
SEISMOMETERS
13
14
15
16
17
18
19
20
21
22
23
24
HYDROPHONES
ACCELEROMETER
26
400 msec

FIG. 8

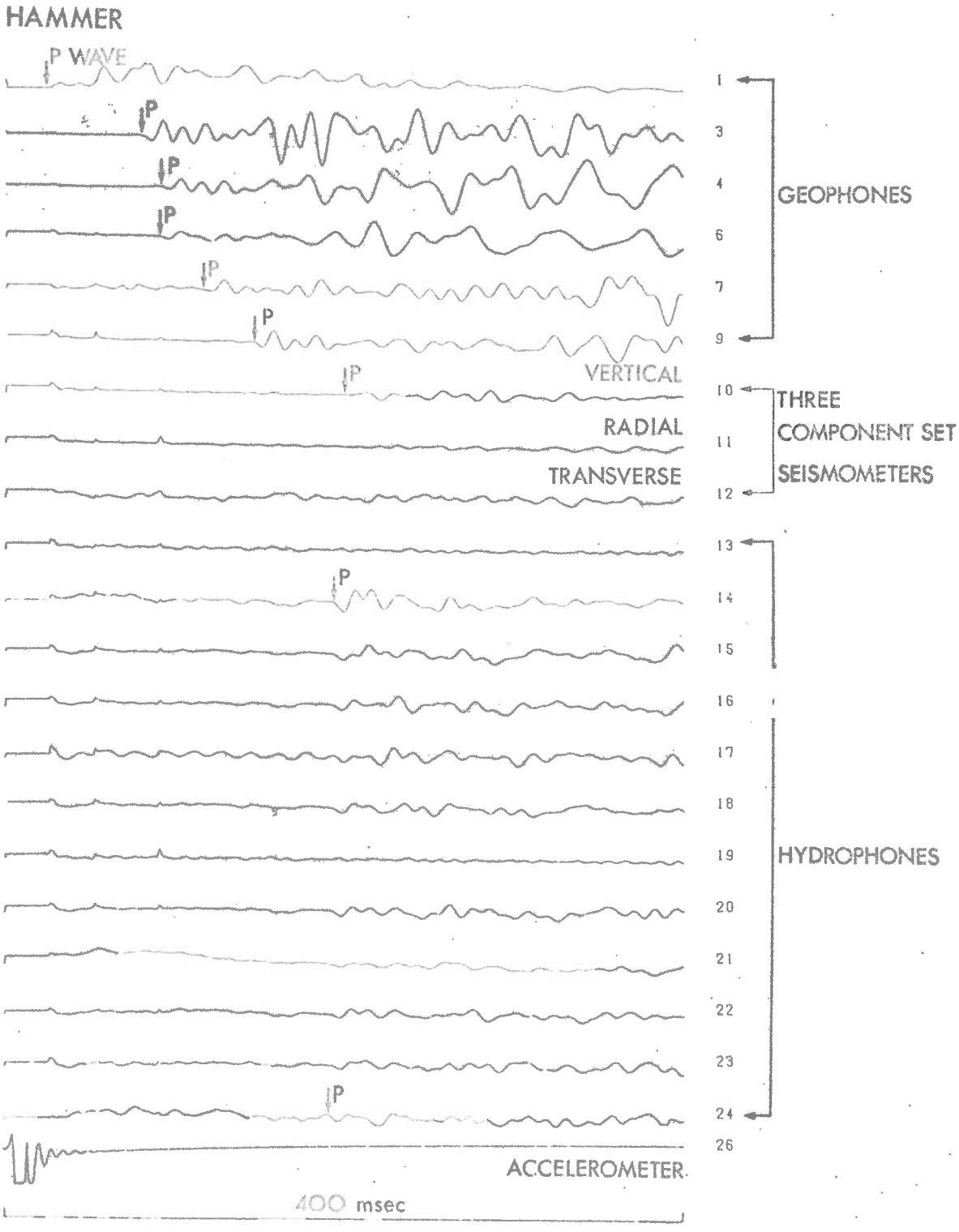
HAMMER
P WAVE
P
VERTICAL
RADIAL
TRANSVERSE
ACCELEROMETER
400 msec
1
3
4
6
7
9
10
11
12
13
14
15
16
17
18
19
20
21
22
23
24
26
GEOPHONES
THREE
COMPONENT SET
SEISMOMETERS
HYDROPHONES

FIG. 9

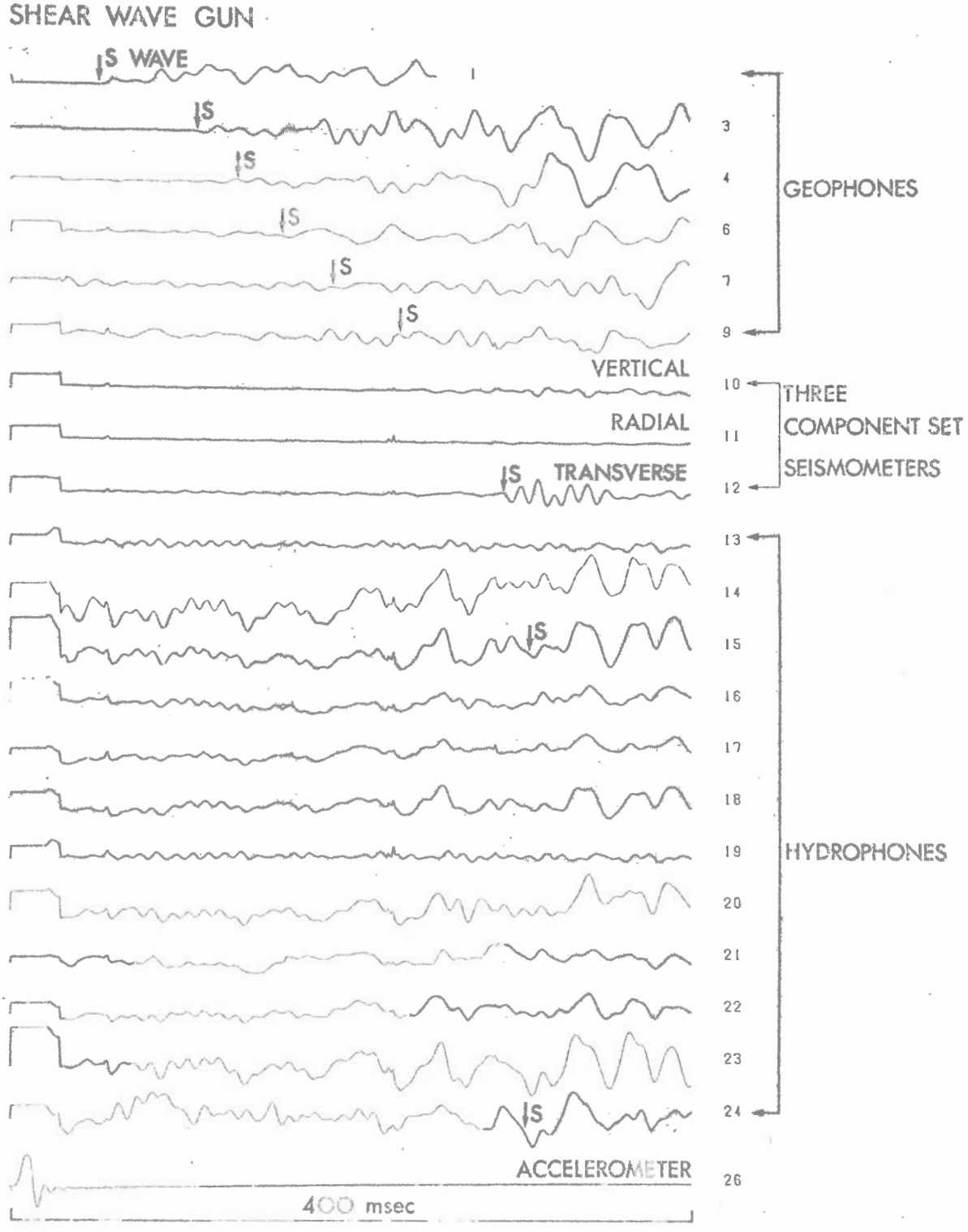
SHEAR WAVE GUN
S WAVE
S
S
S
S
S
VERTICAL
RADIAL
S TRANSVERSE
S
S
ACCELEROMETER
400 msec
3
4
6
7
9
10
11
12
13
14
15
16
17
18
19
20
21
22
23
24
26
GEOPHONES
THREE
COMPONENT SET
SEISMOMETERS
HYDROPHONES

FIG. 10

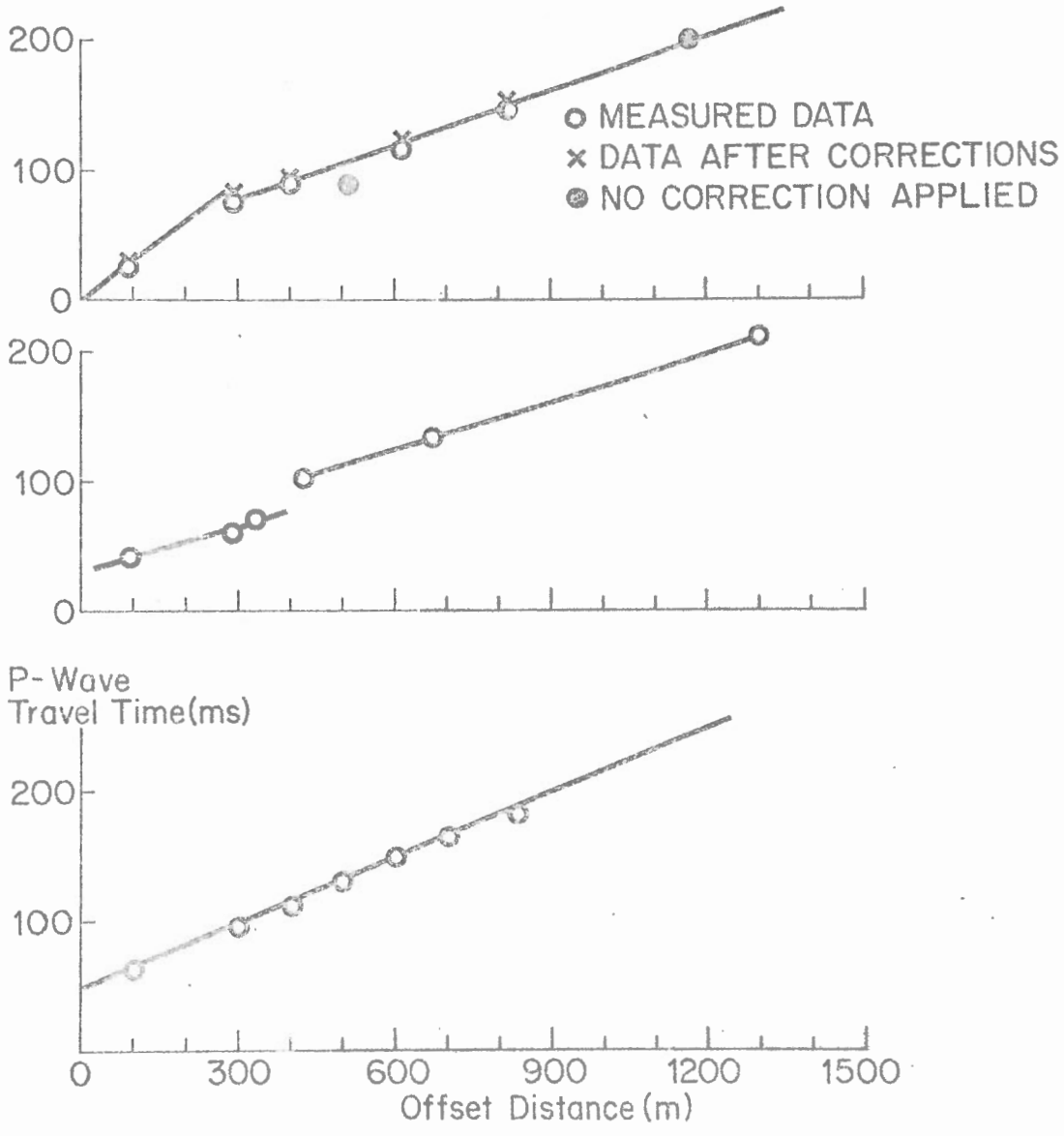
200
100
0
O MEASURED DATA
× DATA AFTER CORRECTIONS
⊗ NO CORRECTION APPLIED
200
100
0
P-Wave
Travel Time(ms)
200
100
0
300
600
900
1200
1500
Offset Distance (m)

Fig. 11

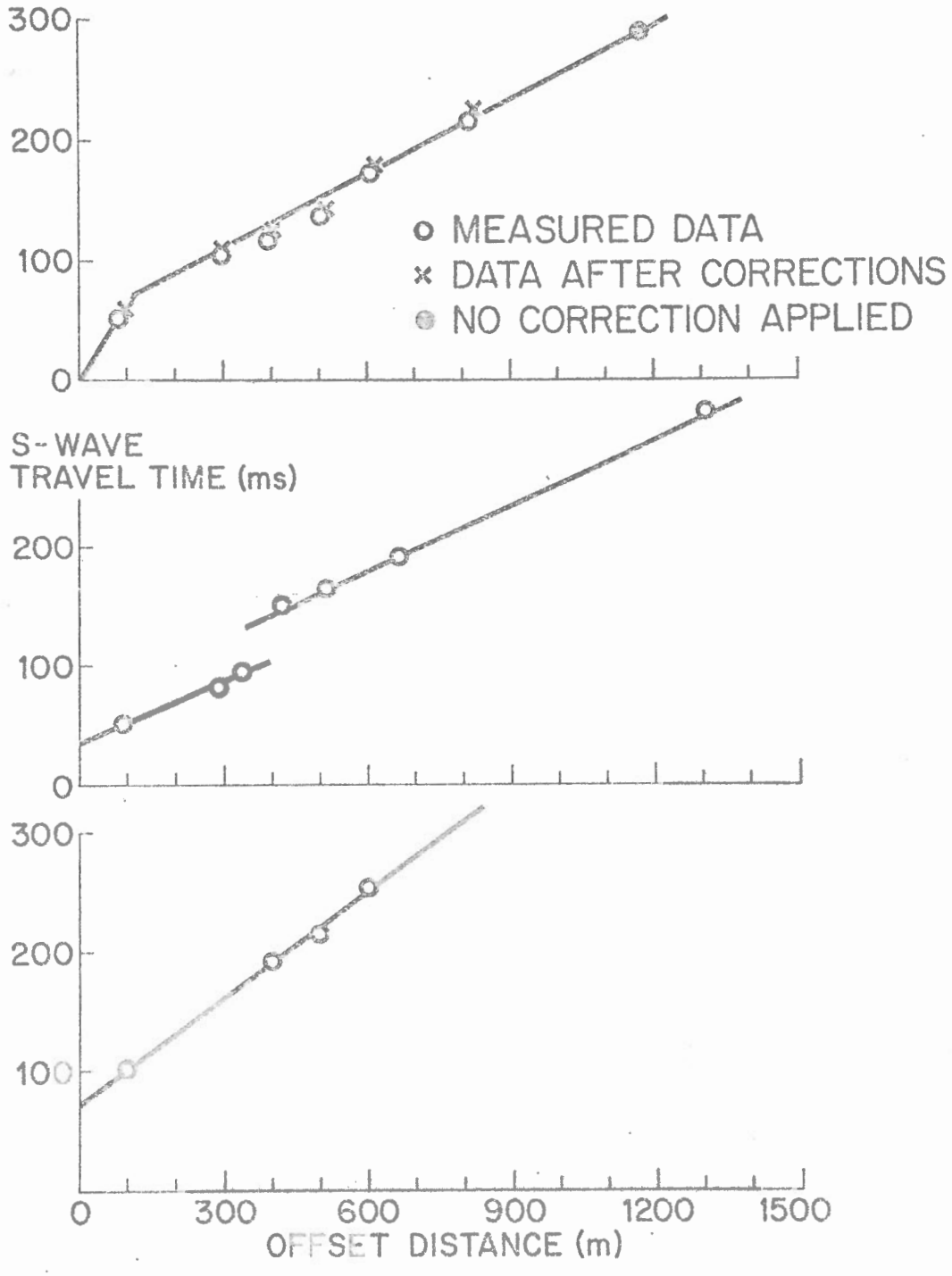
300
200
100
0
o MEASURED DATA
× DATA AFTER CORRECTIONS
NO CORRECTION APPLIED
S-WAVE
TRAVEL TIME (ms)
200
100
0
300
200
100
0
300
600
900
1200
1500
OFFSET DISTANCE (m)

FIG. 12

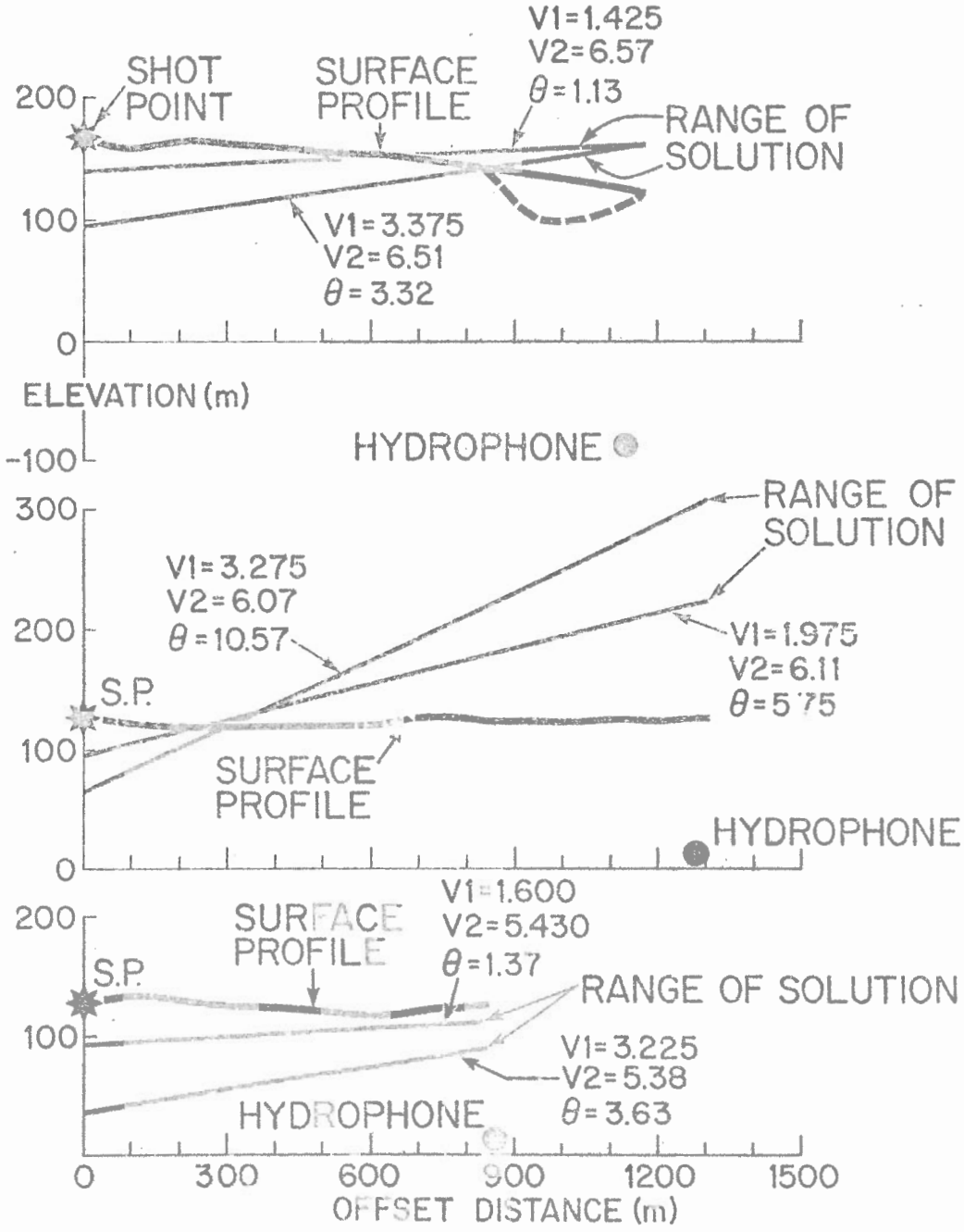
V1=1.425
V2=6.57
θ=1.13
SHOT POINT
SURFACE PROFILE
RANGE OF SOLUTION
200
100
V1=3.375
V2=6.51
θ=3.32
0
ELEVATION (m)
-100
HYDROPHONE
300
RANGE OF SOLUTION
V1=3.275
V2=6.07
θ=10.57
200
V1=1.975
V2=6.11
θ=5.75
S.P.
100
SURFACE PROFILE
HYDROPHONE
0
V1=1.600
V2=5.430
θ=1.37
200
SURFACE PROFILE
S.P.
RANGE OF SOLUTION
100
V1=3.225
V2=5.38
θ=3.63
HYDROPHONE
0
300
600
900
1200
1500
OFFSET DISTANCE (m)

FIG. 13

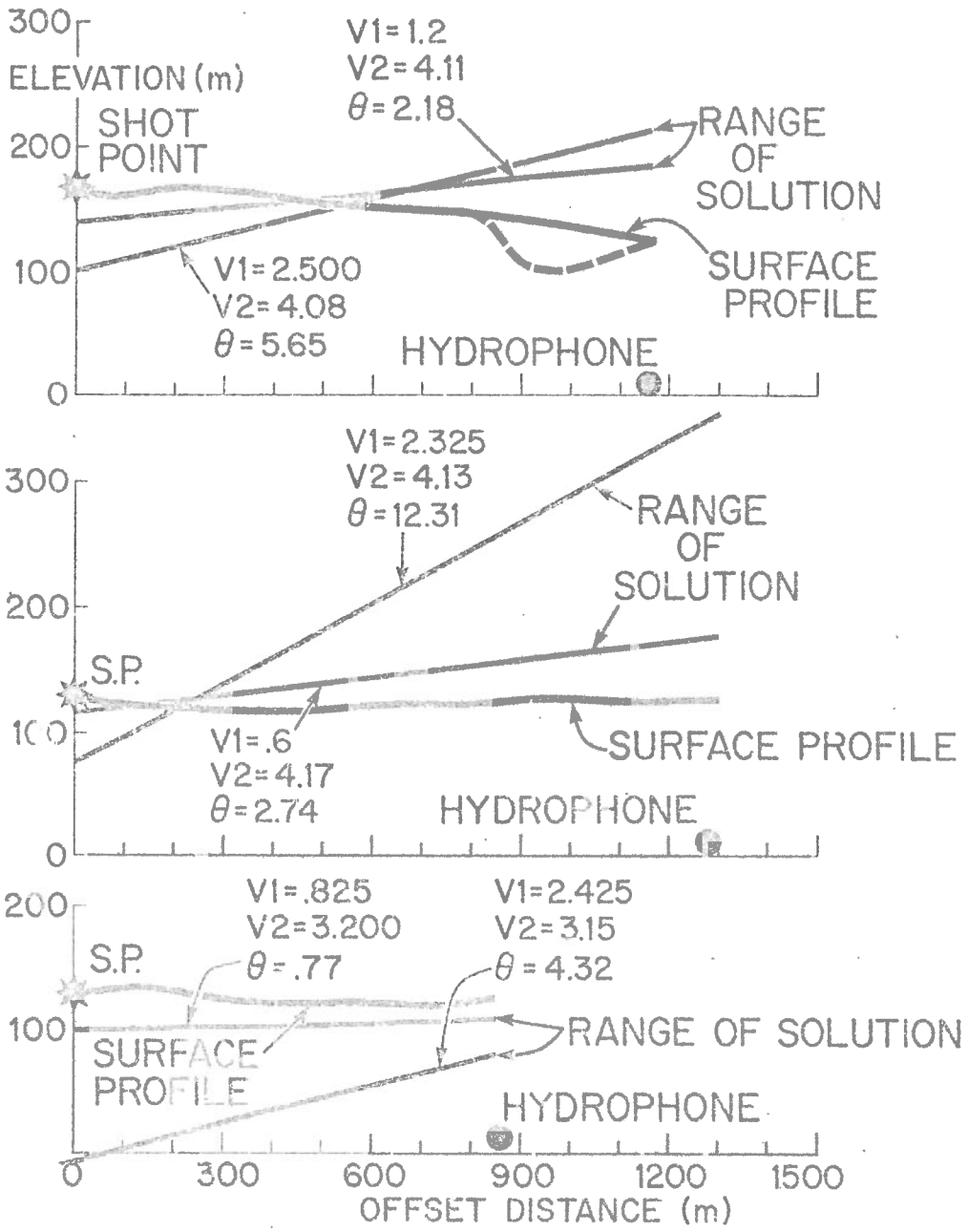
300
ELEVATION (m)
200
SHOT POINT
100
0
V1=1.2
V2=4.11
θ=2.18
RANGE OF SOLUTION
SURFACE PROFILE
V1=2.500
V2=4.08
θ=5.65
HYDROPHONE
300
200
100
0
V1=2.325
V2=4.13
θ=12.31
RANGE OF SOLUTION
S.P.
V1=.6
V2=4.17
θ=2.74
SURFACE PROFILE
HYDROPHONE
200
100
S.P.
V1=.825
V2=3.200
θ=.77
V1=2.425
V2=3.15
θ=4.32
RANGE OF SOLUTION
SURFACE PROFILE
HYDROPHONE
0
300
600
900
1200
1500
OFFSET DISTANCE (m)

Fig 14